1996

Performance comparison of STAP schemes for airborne radar

Zhongxiu Gu
Lehigh University

Gu, Zhongxiu

Performance Comparison of STAP Schemes for Airborne Radar

January 12, 1997

PERFORMANCE COMPARISON OF STAP SCHEMES FOR AIRBORNE RADAR

by
Zhongxiu Gu

A Thesis
Presented to the Graduate Committee
of Lehigh University
in Candidacy for the Degree of
Master of Science
in
Department of Electrical Engineering and Computer Science

Lehigh University
December,1996

This thesis is accepted in partial fulfillment of the requirements for the degree of Master of Science.

12/4/96
(Date)

Rick Blum
(Professor in Charge)

Department Chairperson

Acknowledgments

I would like to thank my advisor Dr. R. S. Blum for his continuous encouragement and for those stimulating discussions. I appreciate this precious chance he has given to me. I also would like to thank Dr. W.L.Melvin for his helpful discussion.

This thesis is based on research sponsored by AFOSR and Rome Laboratory. I want to acknowledge my gratitude to them and I hope more graduate students could be given chance to work in research project.

Finally, I want to thank my family for their always support.

Contents

List of Tables

List of Figures

Abstract

Researchers have developed and examined Space-Time Adaptive Processing (STAP) schemes to cope with the clutter spectral spreading that occurs for a radar mounted on a moving platform. Analysis shows these schemes have great potential. Unfortunately, much of the previous evaluation of STAP algorithms was based on the assumption that accurate estimates of the interference-pulse-noise statistics are available which is usually unrealistic. In this thesis, performance evaluation is based on a highly non-homogeneous environment where interference-plus-noise statistics are unknown. Further, estimates which attempt to characterize the interference-plus-noise environment are obtained by probing nearby range cells which is typical in practice. Often, as we show, these estimates are very inaccurate. A general formulation of a STAP algorithm is defined and several specific cases are described and studied. Both simulated data and real measured radar data are used in the tests. The results indicate that STAP schemes can be developed which will perform well when operating with limited information and possibly mismatched estimates of the interference-plus-noise environment. Further development and study are needed to identify the best STAP schemes for this purpose.

Chapter 1

Introduction

In airborne radar, the detection of targets is often limited by ground clutter and other forms of interference. Platform motion causes Doppler shifts in the ground clutter that makes Doppler filtering alone ineffective. In such cases Space-Time Adaptive Processing (STAP) offers a potential solution.

STAP has been an active research topic for at least the last two decades. Much of the interest was generated by the results in [1] and [2]. Since then several algorithms have been proposed and evaluated using simulated radar data. With the recent improvements in phased array antenna and digital signal processing technology, a STAP-based radar system is becoming an attractive alternative for detection of small airborne targets in severe clutter, as compared to classical low-sidelobe beamforming [3] or displaced phase center arrays.

Current STAP research efforts [4] are focused on, among other things, improved estimation of the clutter-plus-noise statistics, calibrated clutter measurements, real-time processing hardware development, and performance evaluation for the competing STAP approaches. The last one is the interest of this thesis. In most previous research, STAP schemes were evaluated using simulated data or by manipulating fixed platform measurements to simulate motion. While simulated data is very useful in the development and analysis of algorithms, a more complete evaluation includes using actual recorded radar data. Thus, in this thesis, we compare various STAP schemes using both simulated data and actual measured airborne data. A

general STAP processing approach, which includes most linear processing schemes, is developed. This should be useful in designing robust STAP algorithms which is an important topic for future research.

In Chapter 2 we describe the system under consideration and we provide an introduction to STAP. In Chapter 3 we define a general STAP scheme and give a detailed description of several specific approaches. In Chapter 4 we present comparison results which utilize simulated radar data. Comparison results based on measured airborne radar data are presented in Chapter 5. Conclusions are given in Chapter 6.

Chapter 2

System Overview

A radar operates by transmitting energy into the environment and obtaining information concerning the location of objects by detecting reflections of the transmitted energy [5]. Detection of an object requires that the received energy from a reflection be larger than the background energy. There are many contributors to the background energy. The most fundamental one is the random energy fluctuations that result from the random motion of electrons. This contribution is often called noise. The presence of other reflectors, such as the ground, whose energy tends to obscure that of the reflector of interest, can also contribute to background energy. These contributors are denoted as clutter.

Thermal noise [6] is always present in electronic circuits. As the name implies, thermal noise is a function of temperature. For our purpose, an important aspect of thermal noise is that its power spectral density is constant over the bandwidth of typical radar receivers. The effective received noise power P_n due to the combined effects of the antenna and receiver is directly proportional to bandwidth. Thus

$$P_n = kT_sB \tag{2.1}$$

where k is Boltzmann's constant, B is the receiver bandwidth measured in Hz and T_s is the effective temperature of the receiving system.

In military radar applications, an adversary can decrease a radar's detection

capability by inserting a signal in the bandwidth of the radar. This type of interference is known as jamming [3]. Typically, the energy received by the radar due to jamming is far greater than that of thermal noise, so the presence of the jammer can significantly decrease the performance of the radar system. One significant difference between interference due to jamming and thermal noise is that interference due to jamming typically emanates from a single spatial angle, whereas thermal noise has essentially uniform density over spatial angles. Thus, modifying the antenna pattern to ensure a low response in the direction of the jamming will often decrease the effectiveness of the jamming [3].

Clutter [5] can be distributed in angle and range. Further, clutter can be distributed in Doppler frequency. For an airborne surveillance radar, the major source of clutter is ground clutter which is due to the backscattering of radiation from the ground. To detect a target in the presence of clutter with a fixed radar platform, a useful discriminant is that often targets have high velocity, and therefore high Doppler shifts, whereas ground clutter has zero or low velocity, and therefore zero or low Doppler shifts. Delay-line [7] cancelers can be easily configured to have nulls at zero Doppler to suppress this clutter. For moving platforms, Doppler shift is dependent on the aspect angle of a scatter relative to the radar look direction. As a result, this makes the Doppler spectral spread quite large. In order to cancel these aspect-dependent clutter returns, STAP has been found to be useful.

2.1 Radar System

The system under consideration is a pulsed Doppler radar residing on an airborne platform. As defined by the IEEE Standard Radar Definitions [5], a Doppler radar is one which utilizes the Doppler effect to determine the radial component of relative radar-target velocity or to select targets having particular radial velocities. It functions to enhance targets within a particular velocity band while rejecting clutter and other echoes outside the velocity band of interest. When a Doppler radar uses pulsed transmissions, it is called a pulsed Doppler radar.

We assume the radar transmits a coherent burst of M pulses at a constant pulse

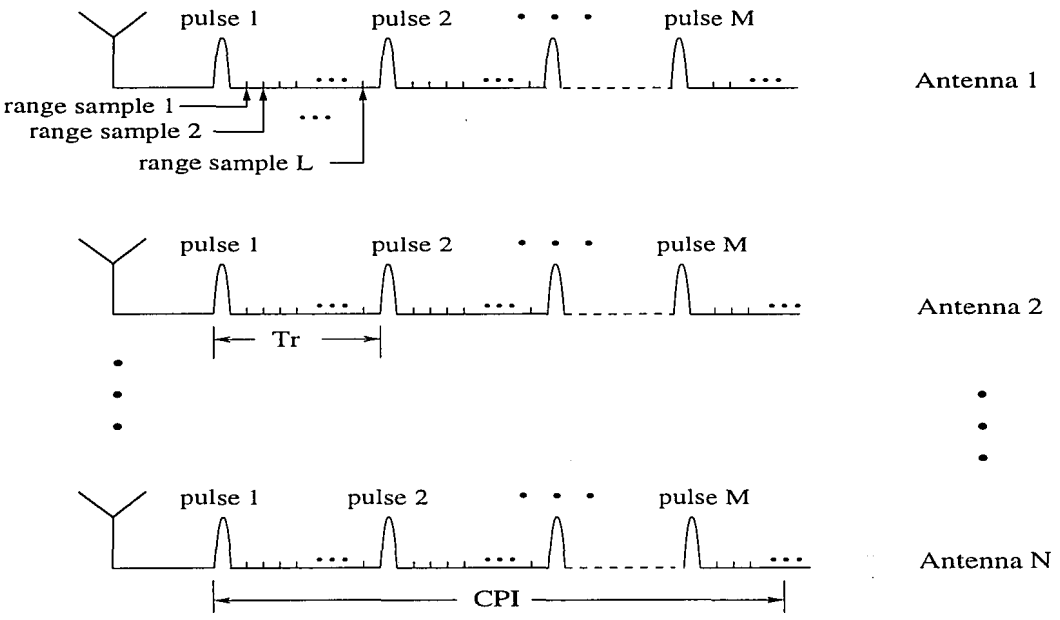

Figure 2.1: Structure of the observed signal returns.

repetition frequency $f_r = 1/T_r$, where T_r is the pulse-repetition-interval (PRI). The time interval over which the waveform returns are collected is commonly referred as coherent-processing-interval (CPI).

In our analysis, the radar antenna used is a uniformly spaced linear array antenna with N identical elements. These elements may be the beamformed columns of a rectangular planar array. It is also assumed that the radar array has a fixed transmit pattern. Each element of the array has its own down-converter, matched filter receiver, and A/D converter. For each PRI, L time samples are collected to cover the range intervals as illustrated in Fig. 2.1.

With M pulses and N antennas, the received data for one CPI comprises LMN complex baseband samples. This multidimensional data set, collected as shown in Fig. 2.1, is often referred as a datacube. Denote the observation corresponding to the i^{th} antenna element at the j^{th} pulse for k^{th} range cell as $x_{i,j,k}$. It is convenient to denote the part of the datacube which represents the k^{th} range cell of the datacube as

$$\mathbf{X}_k = [x_{1,1,k}, x_{2,1,k}, \ldots, x_{N,1,k}, x_{1,2,k}, \ldots x_{N,M,k}]^T \tag{2.2}$$

where a^T denotes the transpose of the vector a. We will refer to $\mathbf{X}_k$ as a space-time snapshot.

As in most analysis of radar systems [8], we assume we can decompose the samples in the datacube as

$$\mathbf{X}_k = \alpha V(S) + X(C) \tag{2.3}$$

where $V(S)$ is the normalized target response, given as

$$V(S) = b(\varpi) \otimes a(\vartheta). \tag{2.4}$$

In (2.4), $\otimes$ denotes the Kronecker product,

$$b(\varpi) = [1, e^{j2\pi\varpi}, \ldots, e^{j(M-1)2\pi\varpi}] \tag{2.5}$$

is an $M \times 1$ temporal steering vector in which ϖ is the normalized target Doppler frequency as defined in [8], and

$$a(\vartheta) = [1, e^{j2\pi\vartheta}, \ldots, e^{j(N-1)2\pi\vartheta}] \tag{2.6}$$

is an $N \times 1$ spatial steering vector in which ϑ is the target spatial frequency as defined in [8]. The symbol $V(S)$ used in (2.4) is often called a target steering vector. In (2.3), α is an unknown constant and $X(C)$ denotes the additive interference-plus-noise returns. $X(C)$ usually consists of additive contributions of clutter, jamming and thermal noise. A typically model for each of the components of $X(C)$ is given in [8].

2.2 Space-Time Adaptive Processing

Most of the STAP schemes that have been suggested can be represented as an inner product of the conjugate of a weight vector w and the vector $\mathbf{X}_k$ which represents the snapshot of interest. This inner product

$$z = w^H \mathbf{X}_k \tag{2.7}$$

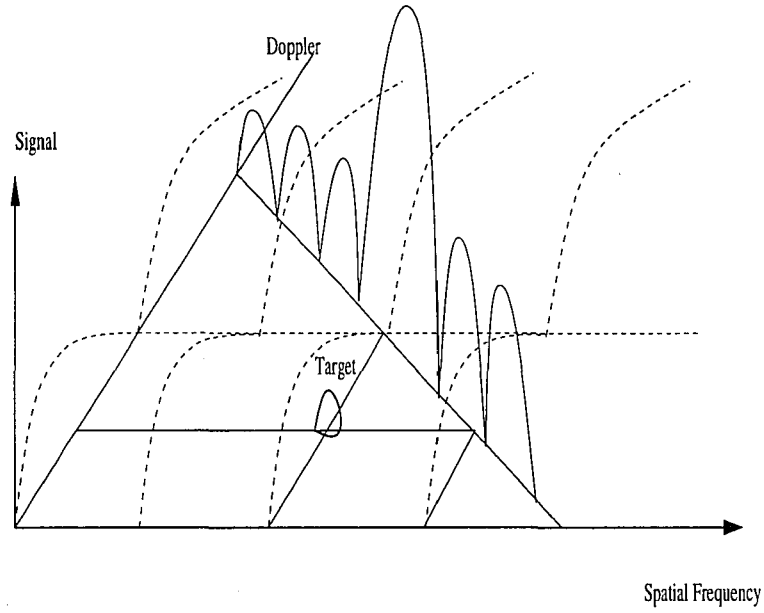

Figure 2.2: One-dimensional Doppler filter applied to ground clutter (adopted from [9]).

produces the complex quantity z whose magnitude is often compared to a threshold to make a decision. The weight vector w may depend on the estimated interference-plus-noise environment and on the target of interest.

One way to view a space-time processor is as a two-dimensional filter. Conventional schemes only use Doppler frequency selectivity and could produce a filtering action as shown in Fig. 2.2. Fig. 2.2 shows the clutter ridge that is characteristic of ground clutter in airborne radar [8]. It is clear that although such a filter can cancel the clutter return due to the mainlobe (assumed to be at zero Doppler) of the antenna response, it is unable to cancel the clutter returns due to sidelobes. STAP schemes combine both the spatial and temporal information and are able to rotate the filter to produce a null along the clutter ridge as shown in Fig. 2.3. Ideally, the space-time processor provides coherent gain for a target while forming angle and Doppler response nulls to suppress interference. As the interference scenario is not known in advance, the weight vector must be determined in a data-adaptive way from the radar returns.

In the well-know sample matrix inversion (SMI) algorithm [2], which is a fully

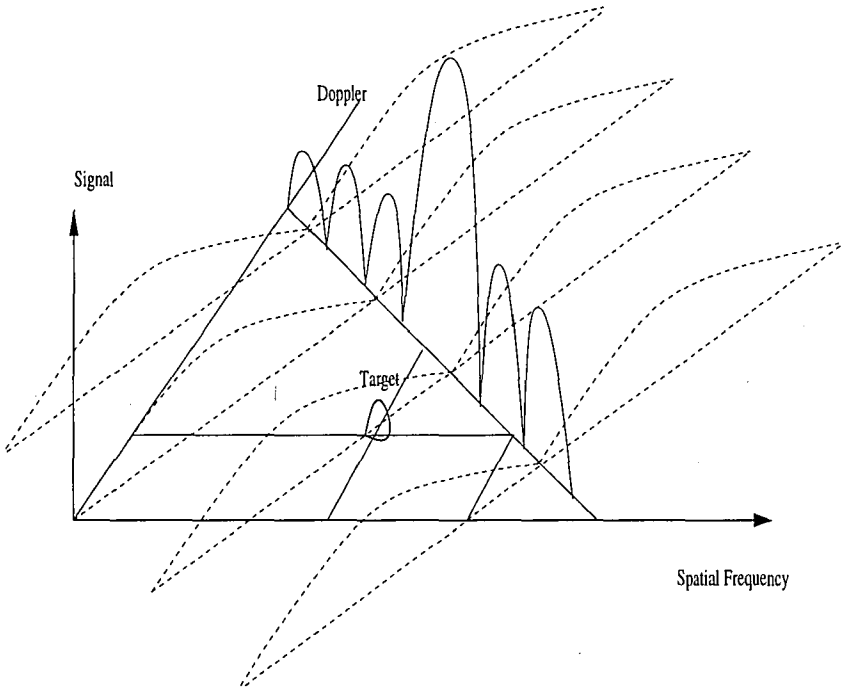

Figure 2.3: Space-time filter applied to ground clutter (adopted from [9]).

adaptive algorithm, the weight vector is given, to within a scale factor, by

$$w = \hat{R}^{-1}V(S) \tag{2.8}$$

where $\hat{R}$ is the estimated interference-plus-noise covariance matrix. The estimate is based on a set of reference data, typically chosen from the surrounding range cells. $V(S)$ is the normalized target response defined in (2.4).

In the case where the interference statistics are known or the estimated covariance matrix is exactly equal to the true covariance matrix, SMI can achieve optimal performance. A fully adaptive STAP scheme is one that requires the formation of an NM by NM covariance matrix which can be a problem. Even for moderate M and N, the computational cost of the estimation and computation of $\hat{R}^{-1}$ becomes excessive in real-time implementations. As a result, reduced complexity approaches have been developed whose computational cost is substantially smaller. Some examples of reduced complexity approaches are given in the next chapter.

The schemes which estimate the interference-plus-noise statistics typically require a large set of independent and identically distributed (iid) reference data

vectors to achieve an accurate estimation. This requirement may be unrealistic, since measurements [10] indicate that multichannel airborne radar clutter data is often severely non-homogeneous. For this reason the reference data set available for estimation of clutter statistics is usually quite small. Therefore it is important to know how different STAP algorithms perform for such cases. A particular STAP algorithm, the adaptive displaced phase-centered antenna (ADPCA) algorithm, appears to provide benefits in some non-homogeneous environment cases where the interference statistics estimates may be inaccurate.

Chapter 3

Some Reduced Complexity STAP Schemes

STAP is an active research area and new schemes are continually being developed. In order to compare schemes, a standard terminology is useful. Here, we will mainly follow the terminology used in [8]. We caution the reader that other terminology also appears in the literature. We first define a general formulation of a for STAP processing approach which encompasses most of existing STAP schemes. We limit consideration to those schemes which linearly combine the space-time observations. Next we describe six specific approaches which are

- Adaptive displaced phase-centered antenna (ADPCA)
- Factored post-Doppler (post-Doppler adaptive beamforming)
- Element-space pre-Doppler
- Beam-space pre-Doppler
- Beam-space post-Doppler
- Joint-domain localized (JDL) approach

each of which are included in the general formulation.

3.1 General STAP Approach

Consider the transformations

$$\widetilde{X}_k(p) = (A_p \otimes B_p)^H \mathbf{X}_k; \quad p = 0, 1, 2, \ldots, P-1 \tag{3.1}$$

where $\mathbf{X}_k$ is the space-time snapshot from the kth range cell and A_p and B_p are scheme-dependent matrices. The operations in (3.1) can be interpreted as a pre-processor applied to the received signals. This preprocessing generates data for the adaptive processing to follow. Note that P vectors are produced by the operations in (3.1). Typically, the pre-processing in (3.1) performs a coordinate transformation and a selection operation.

We describe the adaptive processing on the pth vector produced by (3.1) as

$$\tilde{y}_k(p) = S^H \tilde{R}_k^{-1}(p) \widetilde{X}_k(p) \tag{3.2}$$

where

$$\tilde{R}_k(p) = \frac{1}{Q} \sum_{i=k-Q/2, i\neq k}^{k+Q/2} \widetilde{X}_i(p) \widetilde{X}_i(p)^H \tag{3.3}$$

and S is a scheme-dependent steering vector. $\tilde{R}_k(p)$ is the interference-plus-noise covariance matrix estimated from Q adjacent range cells. Note that (3.2) resembles the SMI scheme defined in (2.7) and (2.8). Further, based on accepted principles, the covariance matrix estimation of an $r \times r$ matrix like $\tilde{R}_k(p)$ nominally requires $Q = 2r$ iid secondary data.

In different schemes, $\tilde{y}_k(p)$ may or may not be the final output of interest. If $\tilde{y}_k(p)$ is the final output of interest, its magnitude will be compared to a threshold to decide if signal is present. For cases where $\tilde{y}_k(p)$ will be processed further, we assemble the complex outputs from each adaptive processor into a $P \times 1$ vector as

$$\tilde{Y}_k = [\tilde{y}_k(0), \tilde{y}_k(1), \cdots, \tilde{y}_k(P-1)] \tag{3.4}$$

and compute

$$\tilde{z}_{k,m} = f_m^H \tilde{Y}_k \tag{3.5}$$

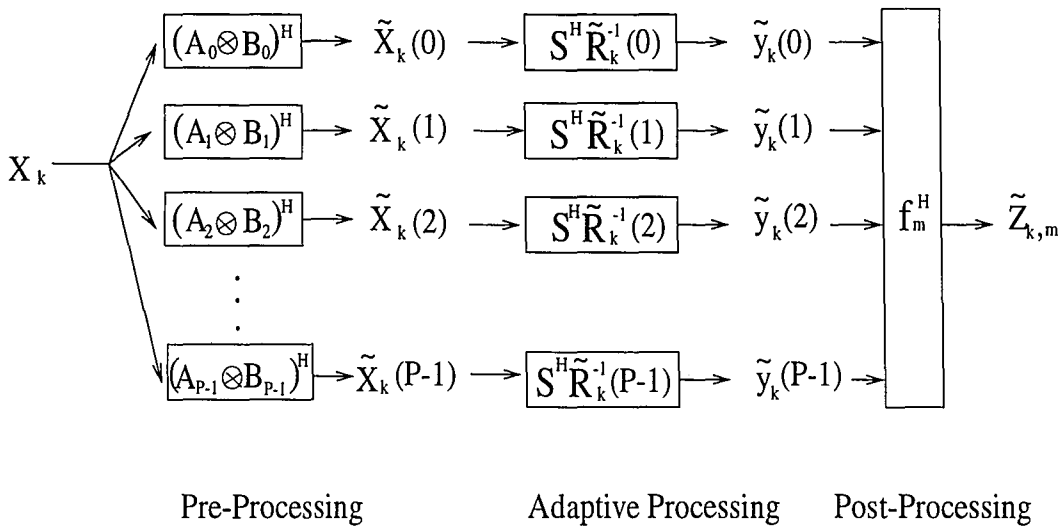

Figure 3.1: Processing flow for a general STAP scheme.

which we call post-processing (after adaptive processing). Typically, f_m is the mth column of a $P \times P$ filter matrix F, and $\tilde{z}_{k,m}$ is the final output whose magnitude will be compared to a threshold to produce a decision. A diagram of the complete processing flow is shown in Fig. 3.1.

3.2 Adaptive Displaced Phase-Centered Antenna

ADPCA is a low complexity alternative to fully adaptive schemes like SMI. ADPCA uses adaptive processing with K_t (typically 2 or 3) pulses at a time rather than all the pulses of the CPI. To be more precise, define a set of P sub-CPIs $\widetilde{X}_k(p), p = 0 \cdots P-1$ in the kth snapshot. Each sub-CPI contains possible signal returns from K_t pulses and all N elements.

Fig. 3.2 shows two different ways to form the sub-CPIs. As indicated in Fig. 3.2, implementation (a) does not overlap pulses. Given M pulses in a CPI where M can be divided by K_t, implementation (a) generates $P = M/K_t$ sub-CPIs. The 0th sub-CPI consists of pulses 0, ..., $K_t - 1$ and the pth sub-CPI consists of pulses pK_t, ..., $pK_t + K_t - 1$. Implementation (b) forms the sub-CPIs by using the same pulse returns in several sub-CPIs. Given M pulses in a CPI, implementation (b)

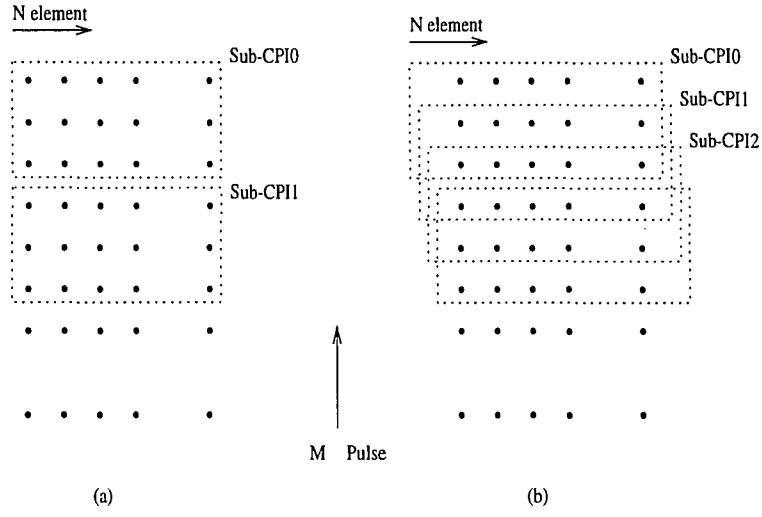

Figure 3.2: ADPCA sub-CPI formation.

generates $P = M - K_t + 1$ sub-CPIs. The 0th sub-CPI consists of pulses 0, ..., $K_t - 1$ and the pth sub-CPI consists of pulses p, ..., $p + K_t - 1$. In Fig. 3.2, K_t is set to 3 and in implementation (b), neighboring sub-CPIs overlap 2 pulses. Of course, other overlaps are possible.

The pre-processing we have just described can be put into the framework of (3.1). B_p is set to I_N which is an $N \times N$ identity matrix and

$$A_p = \begin{bmatrix} 0_{p(K_t-h)\times K_t} \\ I_{K_t} \\ 0_{(M-K_t-pK_t+ph)\times K_t} \end{bmatrix} \tag{3.6}$$

Where the notation $0_{l\times m}$ refers to an $l \times m$ matrix of zeros. h indicates the number of pulses which are overlapped. In implementation (a) h is set to be zero and in implementation (b) h is set to be $K_t - 1$. A_p is an $M \times K_t$ selection matrix.

The adaptive processing in ADPCA is described by (3.2) with the steering vector

$$S = S_t \otimes S_s \tag{3.7}$$

where S_s is the $N \times 1$ spatial steering vector as in (2.6), S_t is a $K_t \times 1$ vector, which is composed of the binomial coefficients, with each coefficient altered in sign (start with positive). As a particular example, we have

$$V_t = (1, -2, 1)^T \tag{3.8}$$

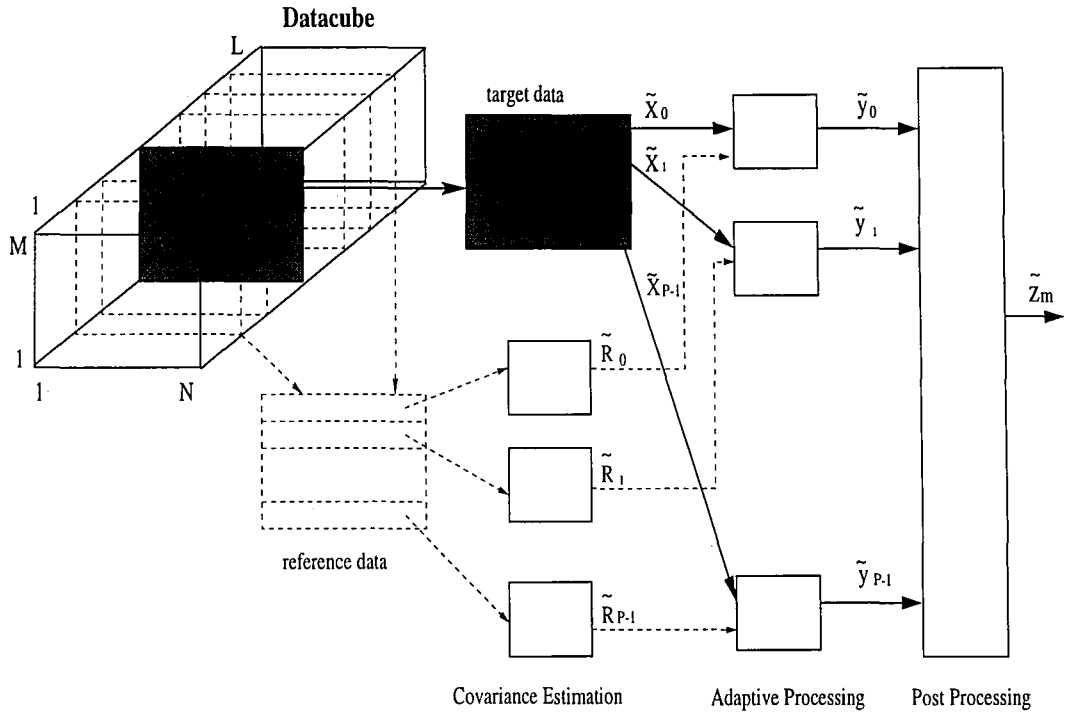

Figure 3.3: Block diagram illustrating the ADPCA algorithm.

for a three pulse case. If $\widetilde{R}_k(p)$ is an identity matrix, and we consider steering to broadside, then application of the ADPCA steering vector has a simple interpretation. At each element, subtract the amplitude of neighboring pulses. Next subtract neighboring results and repeat this process until only a single output is obtained. Finally the outputs from each antenna are summed. It is clear that in this case ADPCA is implementing a pulse differencing scheme which will tend to "whiten" clutter present in the observations.

Typically, post-processing as described in (3.5) is employed in ADPCA. In ADPCA F is a matrix corresponding to a Doppler filter bank, and f_m is the mth Doppler filter. Typically F is DFT matrix and this Doppler processing can then be efficiently implemented by computing an FFT. If adaptive processing completely "whitens" the data, then FFT post processing is optimum. $|\widetilde{z}_{k,m}|$, the final output for Doppler bin m, is compared to a threshold to make a decision if a target is present at this Doppler frequency.

Fig. 3.3 illustrates the principle of the ADPCA processor. One advantage of this

approach is that it allows an accurate estimate of $\tilde{R}_k(p)$ to be obtained with only a small number of reference samples, since the dimensions of $\tilde{R}_k(p)$ are kept small. This can be quite important in practice due to the difficulty in obtaining a large set of homogeneous reference samples [10]. Further, if we assume stationarity returns over the CPI, we can use only one $\tilde{R}_k(p)$ for all p.

3.3 Factored Post-Doppler

In factored post-Doppler STAP [8], Doppler processing is first performed on each spatial channel resulting in a transformed signal matrix. Let the Doppler filter on each element be represented by f_p and for convenience collect the Doppler filters in the $M \times M$ matrix $F_M = [f_0, f_1, \ldots, f_{M-1}]$. Then the pre-processing is described by (3.1) with $A_p = f_p$, $P = M$, and $B_p = I_N$. This pre-processing transforms the signal into Doppler space. In this case p indicates the index of Doppler bin in question. Next, the adaptive processing in (3.2) is employed with the steering vector S defined as in (2.6). As for most of the STAP schemes we discuss, tapering could be applied to the steering vector [8]. Post-processing is not usually employed, so $|\tilde{y}_k(p)|$ is compared to a threshold to test for a target in the pth Doppler bin.

The extended factored approach (EFA) [11] is a slight extension of the factored post-Doppler approach. In EFA, adaptive processing is applied to several adjacent Doppler bins instead of just one. Thus, the pre-processing performs both transformation and selection. In a case where the scheme adapts over 3 adjacent bins, the pre-processing can be described as in (3.1) with $A_p = J_p = [f_{p-1}, f_p, f_{p+1}]$. The other quantities are set the same as in factored post-Doppler STAP. Using EFA as opposed to post-Doppler STAP, will necessarily increase the size of the covariance matrices to be estimated and makes this approach closer to fully adaptive schemes like SMI.

3.4 Element-Space Pre-Doppler

In element-space pre-Doppler STAP [8], the adaptive processing considers only a few pulses at a time. Utilizing more than one pulse provides the temporal adaptivity required for clutter cancelation, while retaining full spatial adaptivity provides a means to handle jamming simultaneously. Clearly this approach is similar to ADPCA in structure. We begin with defining P sub-CPIs each containing signal returns from K_t successive pulses and all elements. As in ADPCA, one could utilize either an overlapped pulse configuration or a non-overlapped pulse configuration (as illustrated in Fig. 3.2). Thus, the pre-processing is described by (3.1) with A_p as described in (3.6) and with $B_p = I_N$. The adaptive processing is described by (3.2) with the steering vector S being a K_t-pulse, N-element normalized target response as in (2.4). Post-processing is usually employed to transform the output into Doppler space. In the standard approach, this post-processing is similar to what was described for ADPCA.

3.5 Beam-Space Pre-Doppler STAP

In beam-space pre-Doppler STAP [8], the dimensionality is reduced in two ways. First, the element data is pre-processed with an $N \times K_s$ beamformer matrix G to produce K_s beam outputs (see [8] for examples and further discussion of the choice of G). Second, only the beam outputs from a K_t-pulse sub-CPI are adaptively processed at one time. Typically $K_t \ll M$ and $K_s \ll N$ so that a significant reduction in problem size is achieved. This pre-processing is described by (3.1) with A_p as defined in (3.6), and $B_p = G$.

The adaptive processing is described by (3.2) with the beam-space steering vector S defined as

$$S = (I_{K_t} \otimes G)^H S_e \tag{3.9}$$

In (3.9), S_e is the steering vector for element-space pre-Doppler STAP. In the standard approach, the post-processing is the same as that described for element-space pre-Doppler.

3.6 Beam-Space Post-Doppler STAP

In the beam-space post-Doppler approach [8], the pre-processing is described by (3.1) with $A_p = J_p$ and $B_p = G$, where J_p is an $M \times K_t$ matrix of Doppler filters. A good example of J_p was that given when we introduced EFA. G is an $M \times K_s$ beamforming matrix similar to that described in Section 3.5. As in factored post-Doppler, the pre-processor transforms the data into Doppler space. The adaptive processing is as defined in (3.2) with the steering vector

$$S = (J_p \otimes G)^H V \tag{3.10}$$

where V is the M-pulse, N-element normalized target response as in (2.4). $\tilde{y}_k(p)$ in (3.2) is the final output for pth Doppler bin. Post-processing is not usually employed.

3.7 Joint-Domain Localized Approach

In the joint-domain localized (JDL) [12] approach, pre-processing transforms data from the space-time domain into the angle-Doppler domain. Then only a few angle-bins covering angles near the target of interest are considered in the adaptive processing. Further, only a few Doppler bins adjacent to the Doppler bin of interest are adaptively processed. Thus, the pre-processor performs two-dimensional transformation and selection. Most conveniently, the transform is the two-dimensional DFT, and the selection picks out a local processing region (LPR) of width L_n in angle and L_m in Doppler.

More precisely, we can define this pre-processing using (3.1) with $A_p = [f_{M,1}, f_{M,2}, \cdots, f_{M,L_m}]$, where $f_{M,i}$ $i = 1 \ldots L_m$, are the columns of an $M \times M$ DFT matrix corresponding to the L_m Doppler bins in the LPR, and with $B_p = [f_{N,1}, f_{N,2}, \cdots, f_{N,L_n}]$, where $f_{N,i}$ $i = 1 \ldots L_n$, are the columns of an $N \times N$ DFT matrix corresponding to the L_n angle bins in the LPR. The adaptive processing can be described as in (3.2). For a uniform PRI and array spacing, the steering vector used in (3.2) has all its entries equal to zero except for the one corresponding to the angle and Doppler bin of the target. No post-processing is employed for JDL.

Chapter 4

Performance Comparison Using Simulations

The performance comparison will be separated into two chapters. In this chapter, theoretically based clutter and noise models are used to described the covariance matrix and hence generate data by computer simulation. A non-homogeneous environment is simulated by choosing an intentional clutter statistics for the mismatch between the reference samples and the clutter statistics for the samples taken from the cell-under-test. In the next chapter, actual measured radar data is used [10].

Consider a simple model [12], which assumes that ground clutter is dominant over other sources of interference. Noise-plus-clutter observations are assumed to consist of additive contributions of noise and clutter and the noise and clutter are assumed to be statistically independent. Furthermore, the noise contribution to the noise-plus-clutter is assumed to be Gaussian distributed and the noise observations at different antenna elements and in different pulses are assumed to be statistically independent. We have obtained very similar results using a more complicated mode [13], but due to the similarity we did not include the results here.

The clutter contributions have a two dimensional power spectral density (psd) as described by [12]

$$P_c(f_t, f_s) = \sum_{d=1}^{K} \frac{\sigma_{c,d}^2}{2\pi\sigma_{ft,d}\sigma_{fs,d}} \exp\left[-\left(\frac{(f_t - f_{ct,d})^2}{2\sigma_{ft,d}^2} + \frac{(f_s - f_{cs,d})^2}{2\sigma_{fs,d}^2}\right)\right] \qquad (4.1)$$

which is a function of Doppler frequency f_t and spatial frequency f_s. The psd in (4.1) consists of K Gaussian-shaped humps, the dth of which is centered at $(f_t, f_s) = (f_{ct,d}, f_{cs,d})$ and has amplitude $\sigma^2_{c,d}$ and a spread in angle and Doppler controlled by $\sigma^2_{ft,d}$ and $\sigma^2_{fs,d}$. The parameters in (4.1) are taken to model the clutter ridge observed in airborne radar. Using this model, we can easily generate mismatched reference data by manipulating parameters in (4.1). In our tests we frequently add one extra hump to the psd corresponding to either the cell-under-test or the reference data. For convenience of reference, we refer to this model as the simple model. Various experiments showed that how the mismatch is generated (whether the extra hump is added in the reference data or added in the cell-under-test and the exact location where the extra hump is added) will influence the relative performance of STAP schemes. Next we present some typical examples.

4.1 Case 1

Consider a case where reference data can be described by the simple model with the parameters set as shown in Table 1 and with $K = 5$. The noise power in

d	$\sigma_{c,d}$	$\sigma_{ft,d}$	$\sigma_{fs,d}$	$f_{ct,d}$	$f_{cs,d}$
1	0.5588	0.01	0.01	-0.35	-0.35
2	0.5588	0.01	0.01	-0.2	-0.2
3	9.9837	0.01	0.01	0.0	0.0
4	0.5588	0.01	0.01	0.2	0.2
5	0.5588	0.01	0.01	0.35	0.35

Table 4.1: Parameters of assumed psd for training samples.

the sample observed at each antenna element and due to each pulse is taken to be 0.001 which gives the clutter-to-noise-ratio $CNR = 50\ dB$. We show the psd of clutter contributions in Fig. 4.1, where the highest peak is from the mainlobe and the rest of peaks represent sidelobes. This simplified clutter spectrum is useful for performance evaluations. It gives a simple representation of the clutter ridge. Assume that the cell-under-test has the same statistics except that its clutter psd

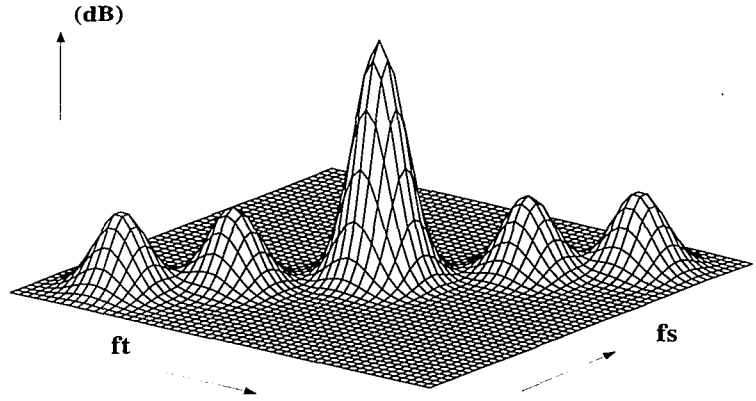

Figure 4.1: Clutter power spectral density for simple model.

includes an additional sixth hump with $\sigma_{c,6} = 2.0$, $\sigma_{ft,6} = 0.01$ and $\sigma_{fs,6} = 0.01$. We present three comparison results and in each of them the sixth hump is added at a different Doppler and spatial frequency. The sixth hump is placed along the clutter ridge at $f_{ct,6} = 0.1$ and $f_{cs,6} = 0.1$, $f_{ct,6} = 0.18$ and $f_{cs,6} = 0.18$, or $f_{ct,6} = 0.3$ and $f_{cs,6} = 0.3$. This type of mismatch could model a case where there is a large clutter return from a few discrete scatters which are not present in the reference data. Such cases have been observed in recently measured airborne data [14]. Alternatively the difference between the psd of the cell-under-test and the psd of the reference data could be the result of false target jamming [4]. For simplicity, a single target is assumed at $\vartheta = 0$ and $\varpi = 0.2$, where ϑ and ϖ are defined in (2.6) and (2.5).

We compare the probability of detection of different STAP schemes as a function of signal-to-interference-plus-noise-ratio (SINR), as discussed in [15]. For each example, two groups of tests are conducted. In group (a), SMI, factored post-Doppler, element-space pre-Doppler, and ADPCA (with two different pulse grouping configurations as shown in Fig. 3.2), are compared for the case where the datacube consists of 2 elements and 12 pulses. In group (b), SMI, beam-space pre-Doppler, beam-space post-Doppler, and ADPCA (with two different pulse grouping configurations)

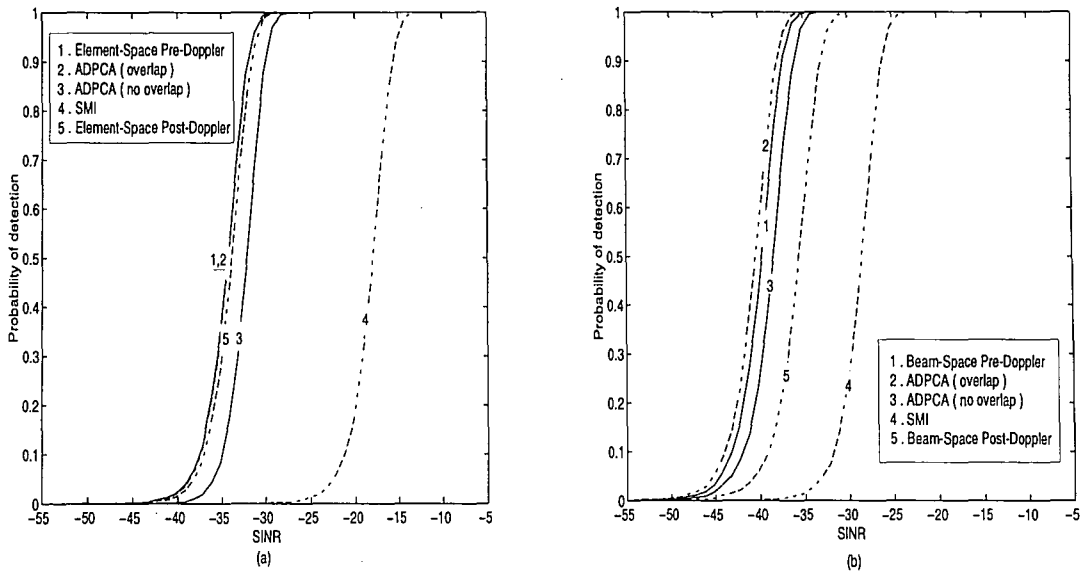

Figure 4.2: Performance comparison for simple model in case 1 with $f_{ct,6} = 0.1$ and $f_{cs,6} = 0.1$.

are compared for the case where the datacube consists of 4 elements and 12 pulses. See Appendix A for the beamforming matrix, as well as for a summary of all the particular parameters chosen.

Fig. 4.2 through Fig. 4.4 illustrate the results. All the results were obtained by setting the true false alarm probability to be $P_f = 0.0001$, and using a Monte Carlo simulation with 10000 runs. Note that in group (b), the datacube includes more pulses than in group (a), so that detection performance is generally improved for all schemes.

4.2 Case 2

Alternatively, mismatch may occur when the psd of the reference data contains an additional hump which does not exist in the psd of the cell-under-test. Assume that the psd for the clutter from cell-under-test has the parameters in Table 1 and that the psd for the reference data contains additional sixth hump with $\sigma_{c,6} = 4.0$, $\sigma_{ft,6} = 0.01$ and $\sigma_{fs,6} = 0.01$. Results are provided for examples where the extra

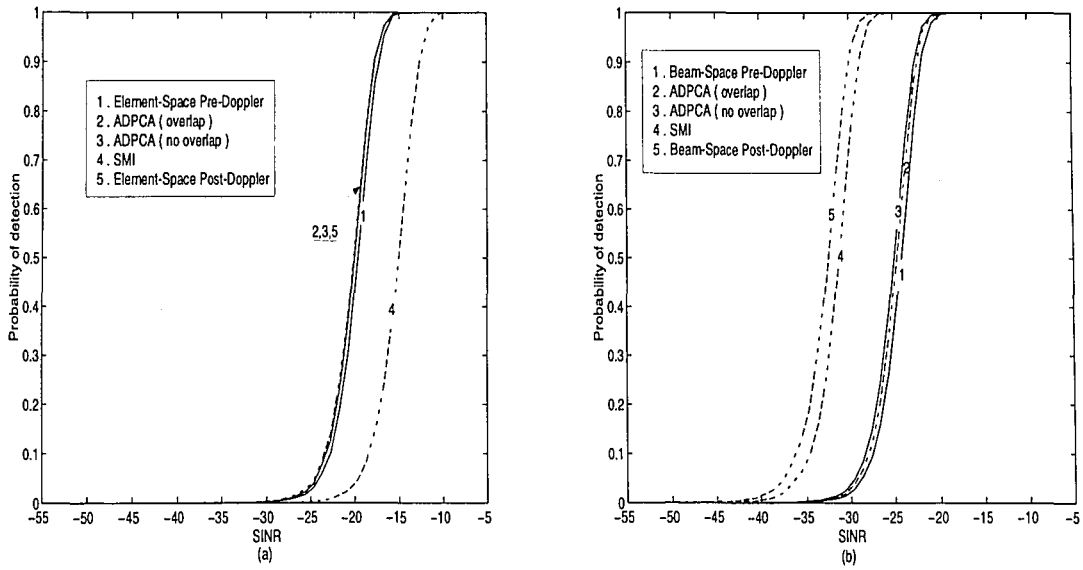

Figure 4.3: Performance comparison for simple model in case 1 with $f_{ct,6} = 0.18$ and $f_{cs,6} = 0.18$.

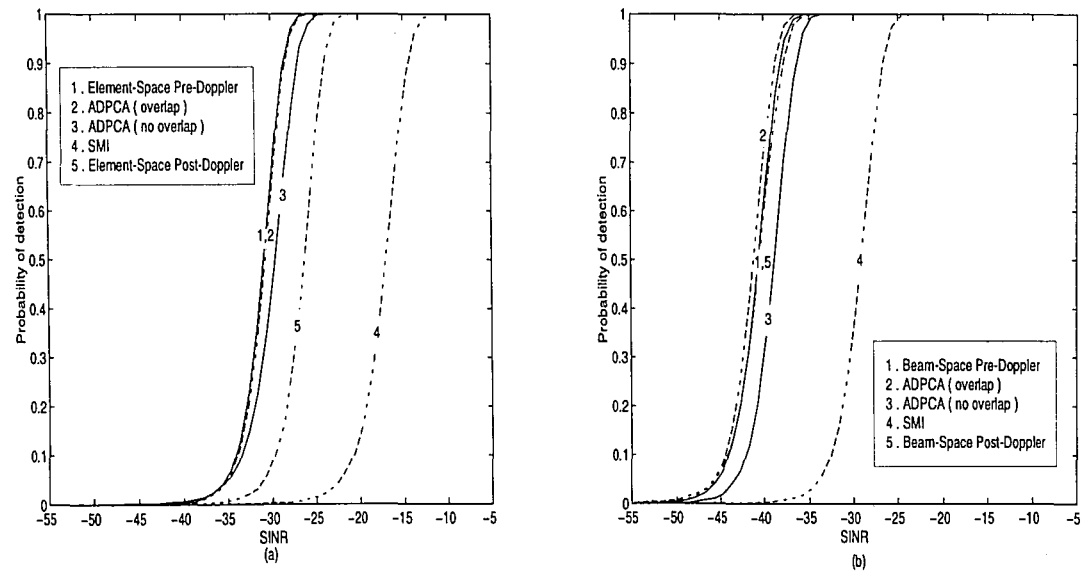

Figure 4.4: Performance comparison for simple model in case 1 with $f_{ct,6} = 0.3$ and $f_{cs,6} = 0.3$.

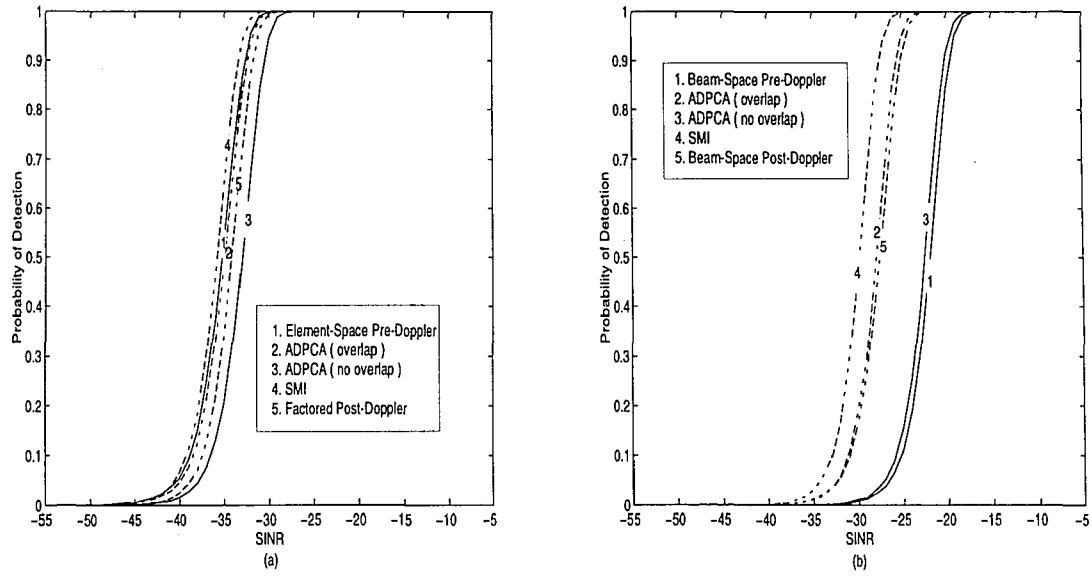

Figure 4.5: Performance comparison for simple model in case 2 with $f_{ct,6} = 0.1$ and $f_{cs,6} = 0.1$.

hump in the psd of the reference data is located at $f_{ct,6} = 0.1$ and $f_{cs,6} = 0.1$, $f_{ct,6} = 0.18$ and $f_{cs,6} = 0.18$, and $f_{ct,6} = 0.3$ and $f_{cs,6} = 0.3$. As in case 1, we assume a single target at $\vartheta = 0$ and $\varpi = 0.2$. Fig. 4.5 through Fig. 4.7 illustrate the results. We conduct two groups of tests under the same condition as described in case 1.

4.3 Discussion of Case 1 and 2 Results

The results indicate that none of the schemes always outperforms all the others. Generally, SMI is not good for a case with mismatch between the reference data and the cell-under-test. If the additional hump is only in the cell-under-test psd then the additional hump is usually not suppressed by the processing. This may be the more common mismatch case. In the other case, where mismatch is due to an additional hump in the reference data psd, things are more complicated. In Fig. 4.5 and Fig. 4.7, SMI outperforms all the other schemes. A possible explanation is that, in the cases of Fig. 4.5 and Fig. 4.7, the reference data has statistics which are a good match to the data from the cell-under-test for angle and Doppler frequencies near the

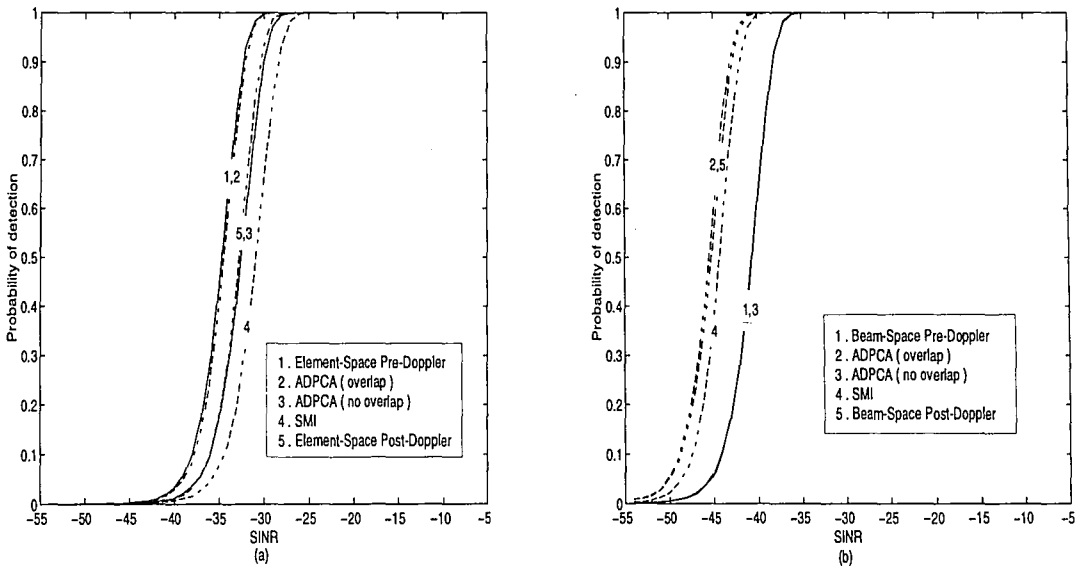

Figure 4.6: Performance comparison for simple model in case 2 with $f_{ct,6} = 0.18$ and $f_{cs,6} = 0.18$.

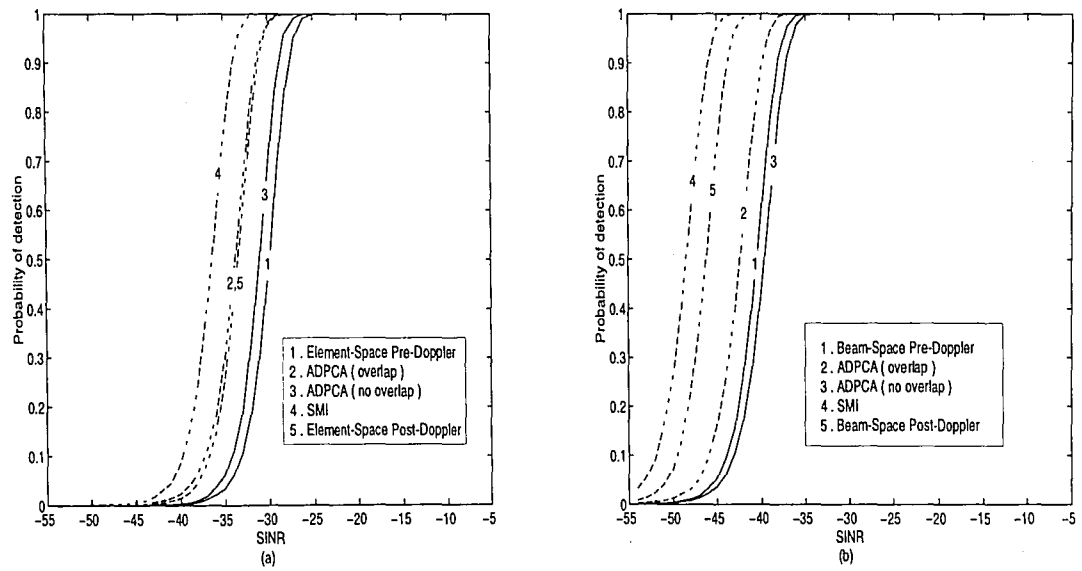

Figure 4.7: Performance comparison for simple model in case 2 with $f_{ct,6} = 0.3$ and $f_{cs,6} = 0.3$.

target. Since the effect of an extra hump is to overly suppress the signal returns from the specific Doppler frequency and spatial frequency where the mismatch located, this won't hurt too much if the target is far from that location. When there is no mismatch between the psd of the reference data and the psd of the data in cell-under-test, SMI is the optimal scheme. This also explained why SMI's performance was degraded in Fig. 4.6. In this case, the target's Doppler frequency is near the mismatch.

ADPCA with overlapped pulses performs well in the most of the cases considered. This is especially true in those comparisons with element-space schemes. Although ADPCA has a similar structure to the element-space pre-Doppler schemes, it usually outperforms them. The reason is apparently based on its pulse canceling structure embedded in its steering vector, which makes it possible to cancel clutter with high correlation across several pulses even if this correlation is not present in the training data. ADPCA without overlapped pulses is not as good as ADPCA with the overlapped pulses. However, in most the cases, the performance difference between the two was not too large. Considering the computation saved, ADPCA without overlapped pulses may still be a good choice in practice. In the results in Fig. 4.3 (b), ADPCA does not perform very well, but in this case none of the pre-Doppler schemes perform very well.

Chapter 5

Performance Comparison Using Measured Data

The multichannel airborne radar measurements (MCARM) program of Rome Laboratory is aimed at accelerating the development of STAP technology through the use of a common set of data. This program provides a database of measured airborne radar data which was collected by Westinghouse during several Delmarva and east coast fly-overs. Data used in this chapter comes from MCARM database flight 5 acquisition 575. Detailed information on the MCARM program and the measurements is available in [10] and [16]. Acquisition 575 includes non-homogeneous clutter. An animation of power spectrum of flight 5 acquisition 575 can be found at http://sunrise.oc.rl.af.mil/java/index.html. We inserted synthetic moving targets into different range bins to compare the detection performance. This performance comparison includes ADPCA, factored post Doppler STAP, EFA and JDL. Reference data are selected from consecutive range cells on each side of the cell-under-test excluding the two closest guard cells. In the ADPCA implementation, each sub-CPI includes 3 consecutive pulses. Further, consecutive sub-CPIs overlap two pulses as shown in Fig. 3.3 (b). In the EFA scheme, adaptive processing is applied to 3 adjacent Doppler bins. In the JDL scheme, we define the LPR as a 3×3 square. See Appendix A for a summary of the parameters chosen for each algorithm tested.

In the first example, we inserted the synthetic target which corresponds to range

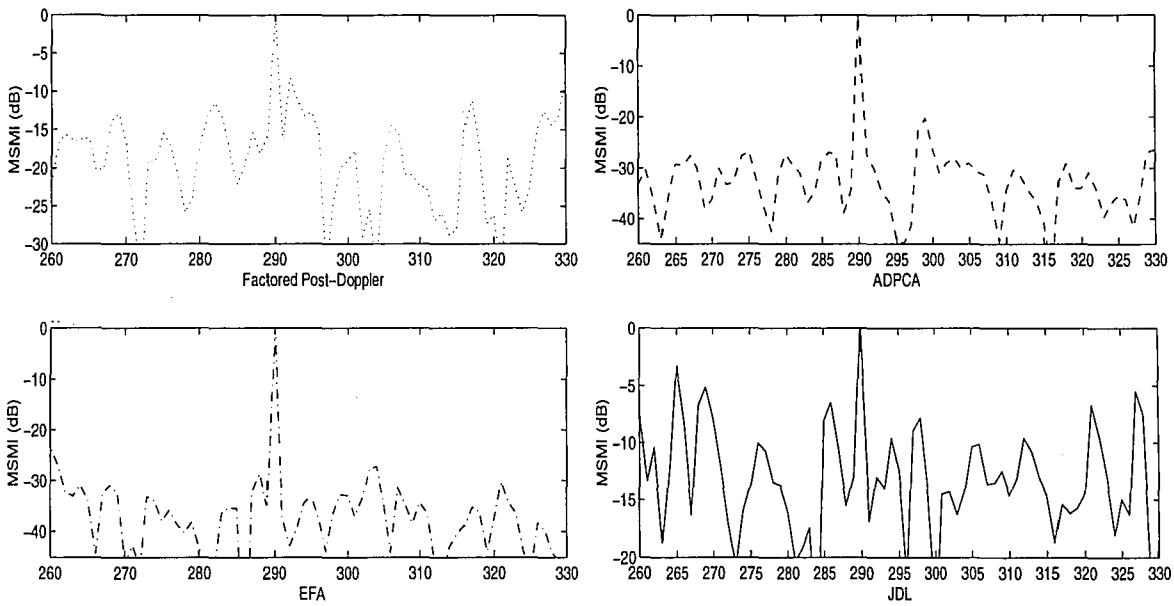

Figure 5.1: Performance comparison for example 1 with Q 3 times the data vector length.

bin 290 and Doppler bin 10. We employ a normalized test statistic (as in [14]) which provides a constant false alarm rate (CFAR) characteristic for homogeneous clutter. Results, in the form of the final test statistic, are provided for different range bins but these results are restricted to Doppler bin 10. In the results which appear in Fig. 5.1, we set the amount of reference data Q to 3 times the data vector length.

To evaluate the impact of the amount of reference data on detection performance, we reduce the amount of reference data Q to twice the data vector length. After the modification, the performance of the different schemes is shown in Fig. 5.2. We further reduce the amount of reference data Q to be equal to the data vector length. We show the performance in Fig. 5.3 for this case.

In the second example, the synthetic target is inserted which corresponds to range bin 415 and Doppler bin 10. Similarly, we provide Fig. 5.4 through Fig. 5.6, which illustrate performance for various Q.

In measured data cases, it is hard to evaluate exactly how the statistics of the reference data and the statistics for the data from the cell-under-test are mismatched. A rough idea can be obtained from considering the energy fluctuation which occurs

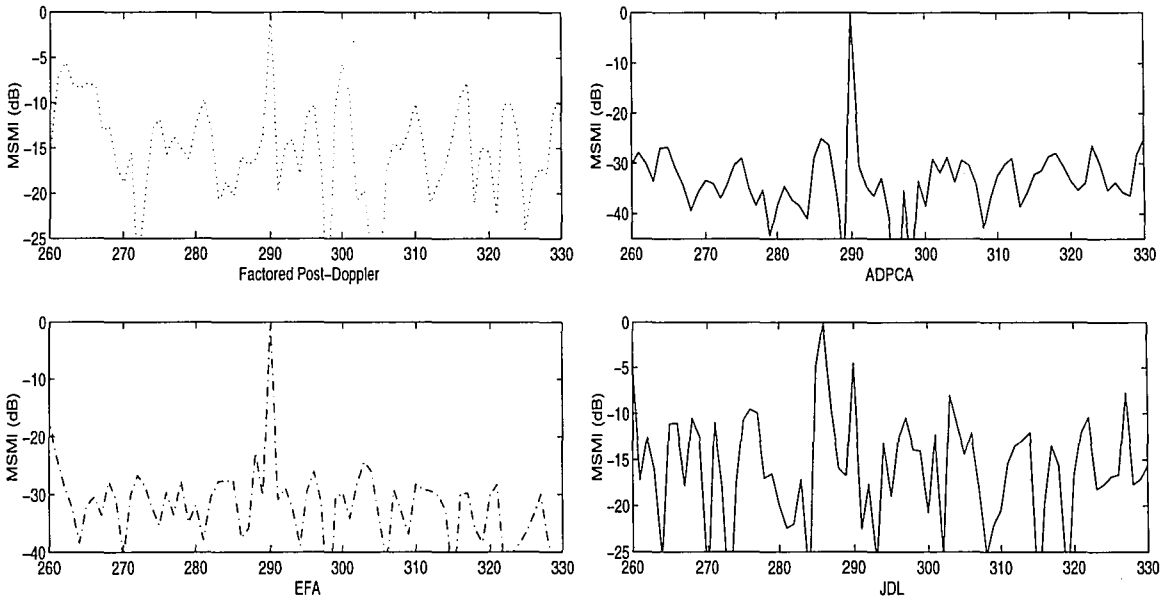

Figure 5.2: Performance comparison for example 1 with Q 2 times the data vector length.

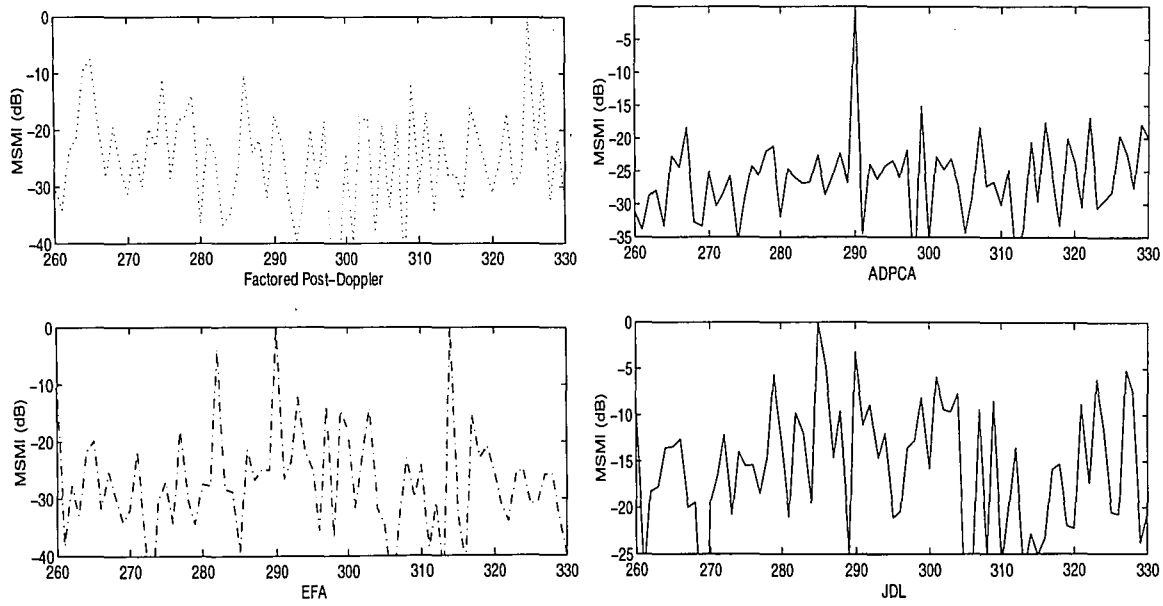

Figure 5.3: Performance comparison for example 1 with Q same as the data vector length.

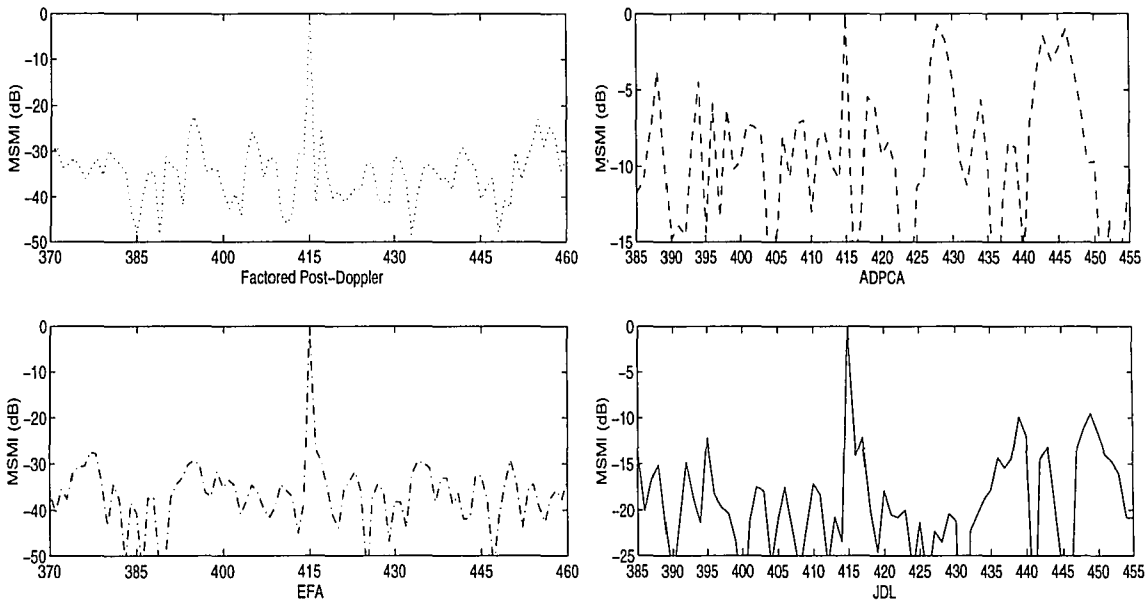

Figure 5.4: Performance comparison for example 2 with Q 3 times the data vector length.

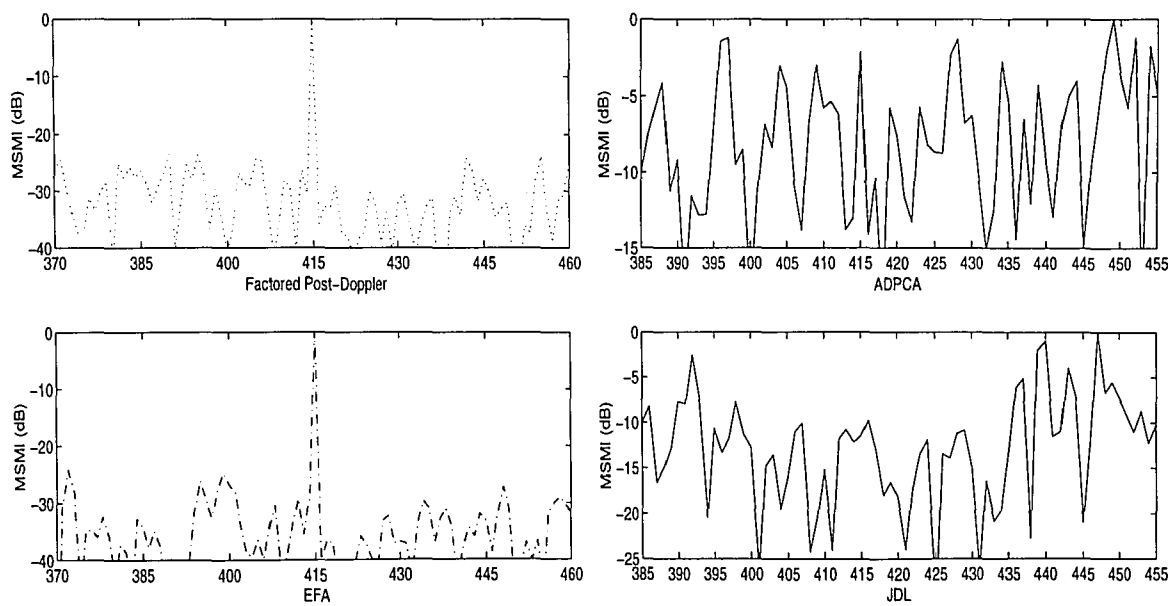

Figure 5.5: Performance comparison for example 2 with Q 2 times the data vector length.

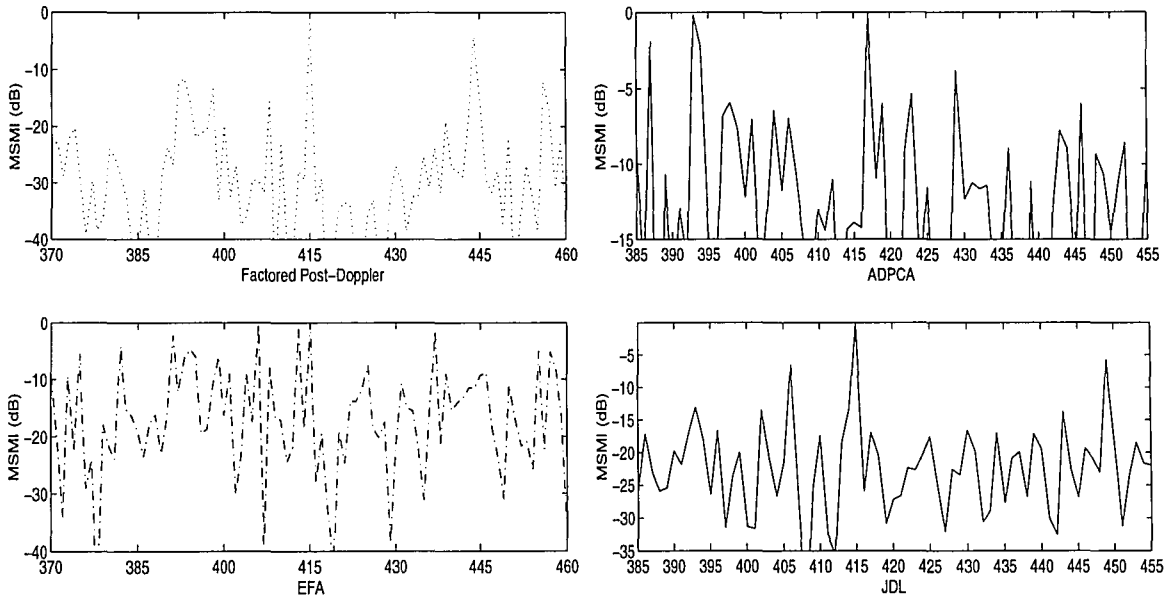

Figure 5.6: Performance comparison for example 2 with Q same as the data vector length.

over range. In Fig. 5.7, we plot the energy in range bin 150 through 400 at Doppler bin 10 with the target signal in example 1. Here the target is located at range bin 290. In Fig. 5.8, we plot the energy in range bin 300 through 550 at Doppler bin 10 with the target signal in example 2. The target in example 2 is located at range bin 415. In Fig. 5.8, there is extreme variation in energy which includes step changes and linear variation in clutter power.

We note that ADPCA appears significantly more robust than EFA, JDL and factored post-Doppler in the results for example 1. Note that ADPCA is not affected significantly by the amount of reference data used. After reducing the amount of reference data used, ADPCA still performs well. The performance of all the other schemes degraded quickly as Q was reduced. To further explore ADPCA's potential, we reduced the amount of computations needed in ADPCA by estimating only one covariance matrix per range bin. We used the covariance matrix estimated for the first sub-CPI for all of the rest of the sub-CPIs corresponding to the same range bin. In this test, we set Q to 3 times the data vector length. As shown in Fig. 5.9 ADPCA still performs very well in this example.

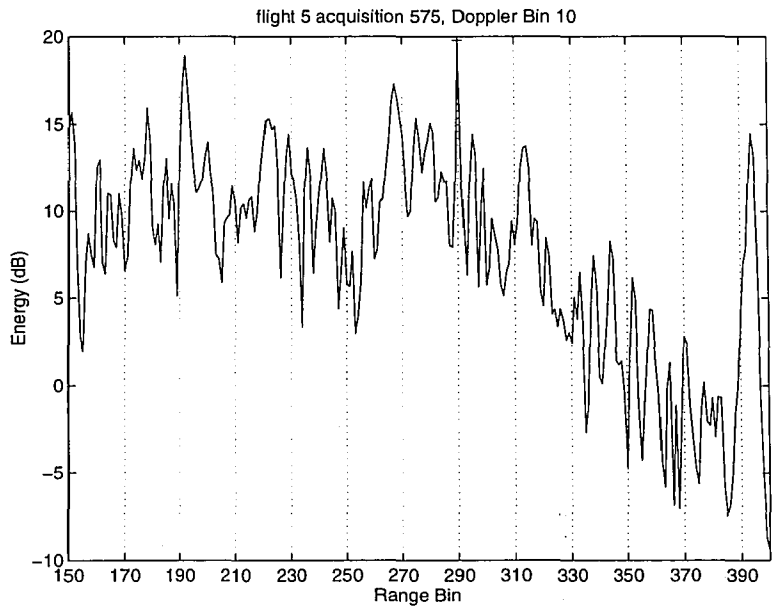

Figure 5.7: Energy for acquisition 575 and range bin 150 through 400 (target at range bin 290).

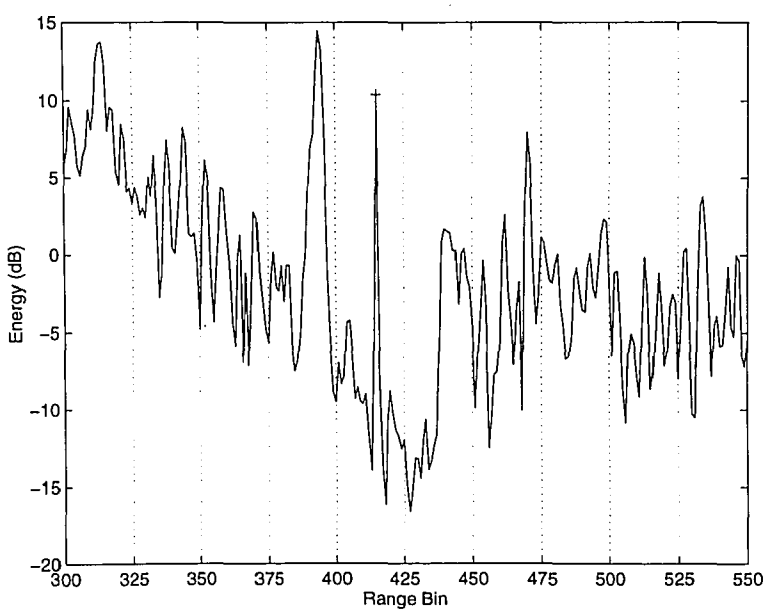

Figure 5.8: Energy for acquisition 575 and range bin 300 through 550 (target at range bin 415).

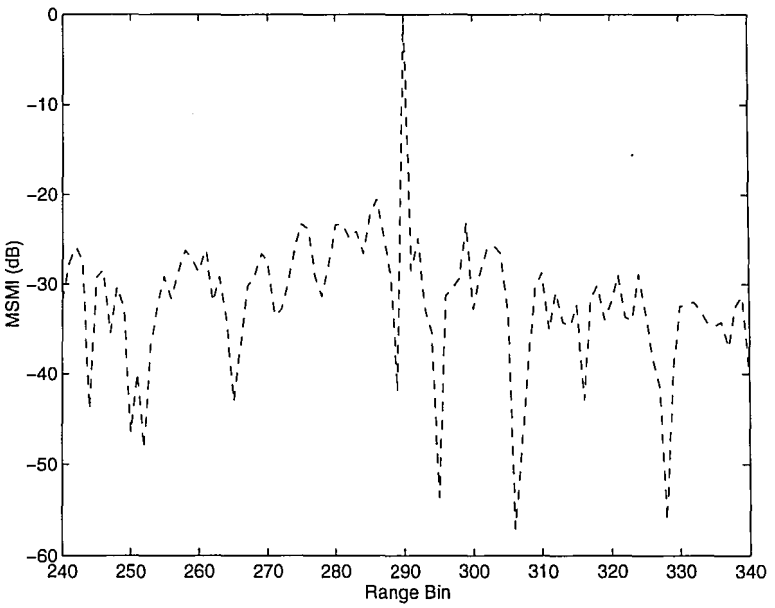

Figure 5.9: ADPCA with reduced complexity for the case where the target at Doppler bin 290.

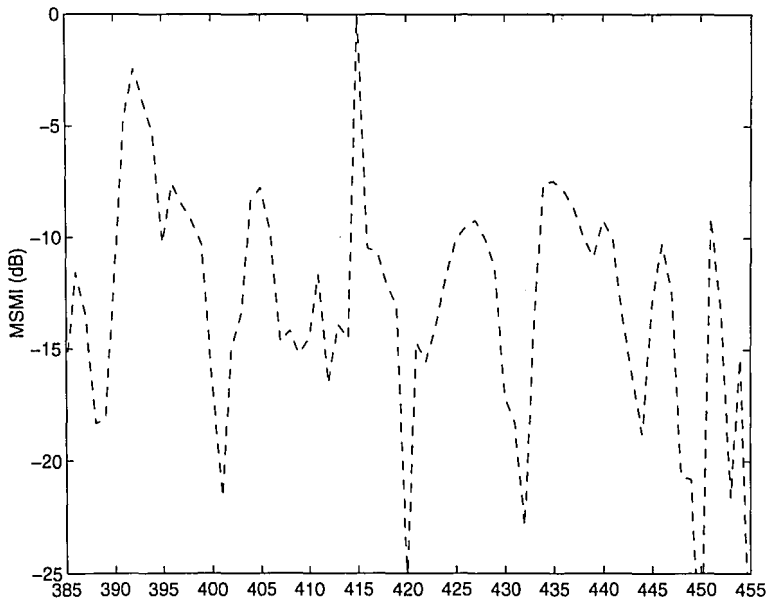

Figure 5.10: ADPCA with reduced complexity for the case where the target at Doppler bin 415.

However, in example 2, ADPCA fails to provide a distinguishable difference between the magnitude of the output at the target bin and the next highest competing clutter peak. Some of the other schemes did work well when there is enough quality reference data. Factored post-Doppler and EFA work well in this example. As in example 1, we tried testing ADPCA's performance when the computation is reduced by estimating one covariance matrix per range bin. Fig. 5.10 illustrates the results. To our surprise, these results are better than the results we obtained before we reduced the amount of computation. Similarly, we find that in Fig. 5.5 and Fig. 5.6 JDL's performance is improved after the amount of reference data is reduced. Reducing the amount of reference data used will not always cause degradation in performance in a severely non-homogeneous clutter environment. This is because the number of homogeneous range samples for covariance estimation is limited. Thus, increasing the amount of reference data used could cause degradation. Actually, it is also the quality of the reference data, not just the amount of the reference data which determines the accuracy of the covariance estimation. In a severely non-homogeneous clutter environment, the situation could be subtle, a small part of the reference data could be dramatically different from the other part and it could distort the estimation. JDL uses the least amount of reference data of all the four schemes under comparison and it seems it is also the one most affected by the change in the amount of reference data. ADPCA does not work well in this example and we believe the reason is related to the step changes in energy near range bin 435 as shown in Fig. 5.8. The normalization of the test statistic which was imposed to achieve CFAR may also have contributed partially to the poor performance of ADPCA and JDL.

Chapter 6

Conclusion

Our results show that the performance of SMI can be severely degraded in a non-homogeneous environment. This is especially true for cases where the reference data used in the estimation of interference-plus-noise statistics does not have statistics which closely match those for the data in the cell-under-test. However, a few STAP schemes appear to outperform SMI in these cases.

ADPCA is one of the promising schemes which performs well in many of the cases studied in this thesis. However, there are some cases where ADPCA performs poorly. Using the knowledge we gained in the current research, we intend to develop generalizations of ADPCA, which will provide even better performance in a practical non-homogeneous clutter environment. One possible approach for developing these generalized schemes is to search for optimal pre-processing and post-processing transformations for cases with inaccurate parameter estimations. Modifying the steering vector so that it can work most effectively with theses transformations would also be interesting to study.

References

1. L. E. Brennan and I. S. Reed, "Theory of Adaptive Radar", *IEEE Trans. on Aerospace and Electronic Systems*, vol. AES-9, no. 2, pp. 237-252, March 1973.

2. I.S.Reed, J.D Mallett and L.E.Brennan, "Rapid convergence rate in adaptive arrays", *IEEE Transactions on Aerospace and Electronic Systems*, AES-10, no.6, November 1974.

3. Alfonso Farina, *Antenna-based Signal Processing Techniques for Radar Systems*, (Artech House: MA, 1992).

4. H. Wang, Y. Zhang and Q. Zhang, "A view of current status of space-time processing algorithm research", *IEEE International Radar Conference*, Alexandria, Virginia, May 1995, pp. 635-640.

5. D. Curtis Schleher, *MTI and Pulsed Doppler Radar*, (Artech House: MA, 1991).

6. Ramon Nitzberg, *Adaptive Signal Processing for Radar*, (Artech House: MA, 1992).

7. Fred E. Nathanson, *Radar Design Principles*, (McGraw-Hill Book Company: New York, 1969).

8. J. Ward, *Space-Time Adaptive Processing for Airborne Radar*, Technical Report 1015, Lincoln Laboratory, 1995.

9. E. C. Barile, R. L. Fante and J. Torres, " Some Limitations on the Effectiveness of Airborne Adaptive Radar", *IEEE Transaction on Aerospace and Electronic Systems*, vol. 28, No. 4, October 1992.

10. D. Sloper et.al., *MCARM Final Rept.*, Rome Lab Tech. Rept., RL-TR-96-49, April 1996.

11. R. C. DiPietro, "Extended Factored Space-Time Processing for Airborne Radar", *Proceedings of the 2th Asilomar Conference*, Pacific Grove CA, October 1992, pp. 425-430.

12. H. Wang and L. Cai, "On adaptive spatial-temporal processing for airborne surveillance radar systems", *IEEE Transactions on Aerospace and Electronic Systems*, Vol. 30, pp. 660-669, July 1994.

13. I. R. Roman and D.W. Davis, *Multichannel System Identification and Detection using output Data Techniques*, Final Report Report No. SSC-TR-96-02.

14. W. L. Melvin, C. Wicks and R. D. Brown, "Assessment of Multichannel Airborne Radar Measurements for Analysis and Design of Space-Time Processing Architectures and Algorithms", *Proceedings of the 1996 IEEE National Radar Conference*, Ann Arbor, MI, May 1996, pp. 130-135.

15. H. Wang, H.R. Pard and M.C. Wicks, "Recent Results in Space-Time Processing", *IEEE International Radar Conference*, Atlanta, Georgia, March 1994, pp. 104-109.

16. W. L. Melvin and B. Himed, "Comparative Analysis of Space-Time Adaptive Algorithms with Measured Airborne Data", *presented at the 7th International Conference on Signal Processing Applications and Technology*, October 7-10, 1996.

Appendix A

Most of the parameters used in the comparisons are listed in the following tables. Here, we use M to denote the number of pulses per CPI, N to denote the number of elements. Definitions of A_p, B_p and f_m can be found in (3.1) and (3.5) where pre-processing and post-processing are defined. We define F_K as a $K \times K$ DFT matrix and $f_{K,p}$ is its pth column. I_r stands for an $r \times r$ identity matrix. The notation $0_{l \times m}$ refers to an $l \times m$ matrix of zeros. Dp is used to denote the Doppler bin where target is located. NA stands for Not Applicable.

Scheme	M	N	p	A_p	B_p	f_m
SMI	12	2	0	I_{12}	I_2	NA
ADPCA (overlap)	12	2	0...9	$\begin{bmatrix} 0_{p\times 3} \\ I_3 \\ 0_{(9-p)\times 3} \end{bmatrix}$	I_2	$f_{10,m}$
ADPCA (without overlap)	12	2	0...3	$\begin{bmatrix} 0_{3p\times 3} \\ I_3 \\ 0_{(9-3p)\times 3} \end{bmatrix}$	I_2	$f_{4,m}$
Element-Space Pre-Doppler	12	2	0...9	$\begin{bmatrix} 0_{p\times 3} \\ I_3 \\ 0_{(9-p)\times 3} \end{bmatrix}$	I_2	$f_{10,m}$
Factored Post-Doppler	12	2	0	$f_{12,Dp}$	I_2	NA

Table A.1: Parameters for comparison tests in Chapter 4 group (a).

Scheme	M	N	p	A_p	B_p	f_m
SMI	12	4	0	I_{12}	I_4	NA
ADPCA (overlap)	12	4	0...9	$\begin{bmatrix} 0_{p\times 3} \\ I_3 \\ 0_{(9-p)\times 3} \end{bmatrix}$	I_4	$f_{10,Dp}$
ADPCA (without overlap)	12	4	0...3	$\begin{bmatrix} 0_{3p\times 3} \\ I_3 \\ 0_{(9-3p)\times 3} \end{bmatrix}$	I_4	$f_{4,Dp}$
Beam-Space Pre-Doppler	12	4	0...9	$\begin{bmatrix} 0_{p\times 3} \\ I_3 \\ 0_{(9-p)\times 3} \end{bmatrix}$	$\begin{bmatrix} 1 & 0 \\ 1 & 1 \\ 1 & 1 \\ 0 & 1 \end{bmatrix}$	$f_{10,Dp}$
Beam-Space Post-Doppler	12	4	0	$f_{12,Dp}$	$\begin{bmatrix} 1 & 0 \\ 1 & 1 \\ 1 & 1 \\ 0 & 1 \end{bmatrix}$	NA

Table A.2: Parameters for comparison tests in Chapter 4 group (b).

Scheme	M	N	p	A_p	B_p	f_m
Factored Post-Doppler	128	22	0	$f_{128,Dp}$	I_{22}	NA
EFA	128	22	0	$[f_{128,Dp-1}, f_{128,Dp}, f_{128,Dp+1}]$	I_{22}	NA
ADPCA	128	22	0...126	$\begin{bmatrix} 0_{p\times 3} \\ I_3 \\ 0_{(125-p)\times 3} \end{bmatrix}$	I_{22}	$f_{126,Dp}$
JDL	128	22	0	$[f_{128,Dp-1}, f_{128,Dp}, f_{128,Dp+1}]$	*	NA

Table A.3: Parameters for comparison tests in Chapter 5.

*MCARM data is not collected by a uniformly spaced linear antenna array, so its beamforming matrix is relatively complicated. This matrix is provided with the MCARM database.

Biography

Zhongxiu Gu was born to Mingyuan Gu and Yanpin Jin on November 1972 in Shanghai, China. She attended Shanghai JiaoTong University since 1991 and graduated with a B.S. degree in Electrical Engineering in 1995.

1. Zhongxiu Gu, Chengang Duan, and Zhihang Zhen, "Using Genetic Algorithm for Motion Estimation" *Accepted in press on Journal of Shanghai Jiao Tong University.*

END

OF

TITLE